Preparation of functional nanoparticles of mPEG - b - P (DMA - co - HA) copolymers via polymerization-induced thermal self-assembly

Akar, Irem; Pearce, Amanda K.; Kumar, C. M. Santosh; Ferguson, Calum; O'Reilly, Rachel K.

DOI:
10.1002/pol.20230420

Document Version
Publisher's PDF, also known as Version of record

Citation for published version (Harvard):
Akar, I, Pearce, AK, Kumar, CMS, Ferguson, C & O'Reilly, RK 2023, 'Preparation of functional nanoparticles of mPEG - b - P (DMA - co - HA) copolymers via polymerization-induced thermal self-assembly', *Journal of Polymer Science*. https://doi.org/10.1002/pol.20230420

Received: 21 June 2023 | Revised: 5 August 2023 | Accepted: 5 August 2023

DOI: 10.1002/pol.20230420

RESEARCH ARTICLE

JOURNAL OF POLYMER SCIENCE WILEY

Preparation of functional nanoparticles of mPEG-*b*-P(DMA-*co*-HA) copolymers via polymerization-induced thermal self-assembly

Irem Akar[1] | **Amanda K. Pearce**[1] | **C. M. Santosh Kumar**[2] | **Calum Ferguson**[3] | **Rachel K. O'Reilly**[1]

[1]School of Chemistry, University of Birmingham, Birmingham, UK

[2]School of Biosciences, University of Birmingham, Birmingham, UK

[3]Max Planck Institute for Polymer Research, Mainz, Germany

Correspondence
Rachel K. O'Reilly, School of Chemistry, University of Birmingham, Edgbaston, Birmingham, B15 2TT, UK.
Email: r.oreilly@bham.ac.uk

Abstract

Self-assembled polymeric nanoparticles have been of great interest for various biological applications such as drug delivery, catalysis, and biosensing. In this regard, polymerization-induced self-assembly (PISA) has been widely explored as a more efficient technique than conventional self-assembly methods as it can be conducted in one pot and does not require harsh conditions. Recently, a method known as polymerization-induced thermal self-assembly (PITSA) has emerged, exploiting the inherent phase transition behavior of thermoresponsive polymers at a critical temperature point to generate thermoresponsive nanoparticles in situ. However, the narrow range of monomers suitable for PITSA limits the design of diverse thermoresponsive nanoparticles, and therefore this process has not yet been explored to its fullest capacity. In this study, we demonstrate the preparation of thermoresponsive nanoparticles based on hydrophilic *N,N*-dimethyl acrylamide (DMA) and hydrophobic hexyl acrylate (HA) monomers. This is particularly interesting as these monomers produce non-responsive homopolymers but display thermoresponsive behavior when copolymerized. The nanoparticles obtained were crosslinked to enable their characterization at room temperature, and further functionalized with a short synthetic antibacterial peptide $(WR)_3$ to demonstrate proof-of-concept potential as antimicrobial agents. Overall, this work expands the library of monomers amenable to PITSA for the production of thermoresponsive nanoparticles, contributing to the design of new functional nanoparticles for therapeutic purposes.

KEYWORDS

nanoparticles, polymerization-induced thermal self-assembly, thermoresponsive polymers

1 | INTRODUCTION

Self-assembled polymeric nanoparticles have garnered increasing attention over the past decades as these nanoparticles have been used for a wide range of applications such as drug delivery vehicles, sensors, catalysts, and coating materials.[1–5] Having the ability to modify their structure by tuning their compositions and/or

functionalize them with small molecules renders them powerful tools for therapeutic applications.[6] Recent advances in reversible deactivation radical polymerizations have further aided the preparation of self-assembled polymeric nanoparticles, enabling their engineering by precisely controlling the different constituents in polymer structures.[7,8] This in turn influences the size, shape, and morphology of the final nanoparticles, facilitating the preparation of diverse self-assembled polymeric systems.[9]

Conventional self-assembly methods such as solvent switch, direct dissolution and thin-film rehydration have been widely used for the formation of nanoparticles.[10] However, there are several drawbacks, including time-consuming multi-step procedures such as synthesis and purification of polymers prior to self-assembly, and the requirement of dilute polymerization solutions for self-assembly to occur.[8] More recently, the advent of polymerization-induced self-assembly (PISA) has addressed many of these challenges. PISA is a one-pot reaction that can be conducted under mild conditions and in organic solvents and water, can be performed at high solids content (up to 50% w/w) and does not require the use of surfactants. For dispersion polymerization mediated PISA, a water-soluble macro-chain-transfer agent is chain extended with water miscible monomers in an aqueous system and becomes progressively more hydrophobic as the polymerization proceeds to form an amphiphilic block copolymer composing of a soluble and an insoluble chain. This leads the insoluble chains in water to self-assemble, forming nanoparticles.[8,11,12]

"Smart" polymers that can change their properties upon exposure to external stimuli have been proven to be great tools for therapeutic applications.[13] Here, polymers can be functionalized by incorporating certain moieties that respond to external stimuli such as light, pH, redox and temperature.[13–17] If formulated into nanoparticles, upon applying the stimuli, polymer chains can undergo a physical or chemical change affecting the resulting nanoparticle structure.[18] Temperature has been the most widely studied of these stimuli as it is easily applicable externally, and is tunable *via* many methods within the desired range to create the required thermoresponse.[17] Thermoresponsive polymers display unique behavior in water known as lower critical solution temperature (LCST) or upper critical solution temperature (UCST), whereby a phase transition occurs above or below a certain temperature point for LCST and UCST behavior, respectively.[19] Since the transition happens at high temperatures in the case of UCST, LCST polymers are preferable for biological applications, as the physiological temperature range can be targeted easily with LCST polymers.[20] The strong interactions between polymer chains and solvent allow polymers to be soluble below their LCST. The phase transition then occurs upon heating above a certain temperature leading to the polymer chains becoming immiscible as the polymer-solvent interactions weaken.[21–23]

The ability to tune the LCST behavior is another advantage that makes thermoresponsive polymers attractive for many applications. A variety of methods have been reported to achieve this, such as changing polymer solution concentration, molecular weight, and hydrophobicity.[24–26] Tuning polymer hydrophobicity is particularly interesting, as this can readily alter polymer-solvent interactions.[27] There are several ways to tune the polymer hydrophobicity, such as altering the polymer structure or using copolymerization. Kempe and coworkers reported that the overall polymer hydrophobicity of graft copolymers could be increased by increasing the length of the side chains, thereby decreasing polymer LCST.[28] Several groups including Lutz, Hoth, Kostjuk, Georgiou, and ourselves, have previously reported that polymer LCST could be controlled by copolymerizing with a high LCST monomer with monomers of lower LCST.[29–33] Recent reports by our group have also shown that the thermoresponsive behavior of amphiphilic copolymers can be tuned by diversifying the hydrophobicity of comonomers in both brushy and linear copolymers.[34] In the case of linear polymers, it was also shown that the thermoresponsive behavior of the polymers could be correlated to their hydrophobicity.[35]

The abundance of methods for tuning polymer thermoresponsiveness, as well as their facile production *via* reversible deactivation radical polymerization techniques, has led to these polymers being widely investigated. A recent technique that combines the advantages of thermoresponsive polymers with the versatility of PISA has been denoted as polymerization-induced thermal self-assembly (PITSA), and was first reported by Sumerlin and coworkers.[36] During PITSA, polymer chains self-assemble once they reach critical length, upon which they become hydrophobic, then proceed to follow the same mechanism as PISA. The entropic changes in the system contribute to the self-assembly process as this drives the phase transition of polymer chains once the system reaches a critical temperature.[36,37] For example, Sumerlin and coworkers reported PITSA of a well-known thermoresponsive monomer *N*-isopropylacrylamide (NIPAM) using a hydrophilic chain transfer agent of *N, N*-dimethylacrylamide (DMA). Here, they reported the evolution of morphologies from micelles to a micelle/worm mixture, to worms and finally to vesicles as the NIPAM polymerizes.[36]

Inspired by this work, we wanted to investigate whether we could expand the library of available monomers for the production of thermoresponsive nanoparticles via PITSA to be able to more extensively utilize the advantage of inherent phase transition behavior of thermoresponsive polymers. Our previous study reports the

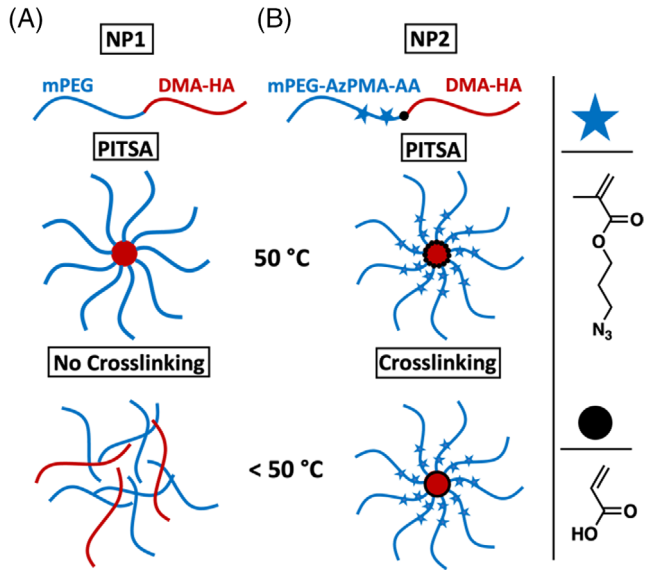

FIGURE 1 Schematic representation of the preparation of (A) uncrosslinked mPEG-*b*-P(DMA-*co*-HA) nanoparticles (**NP1**) and (B) crosslinked mPEG-*b*-P(AzPMA)-*b*-P(AzPMA-*co*-AA)-*b*-P(DMA-*co*-HA) nanoparticles (**NP2**).

production of thermoresponsive polymers by copolymerizing non-responsive *N*,*N*-dimethyl acrylamide (DMA) and alkyl acrylates. In particular, we sought to validate that this behavior would translate into a self-assembly process during PITSA, as this would provide an insight for the design of new thermoresponsive nanoparticles using monomers that produce non-responsive homopolymers. With this goal, we selected hydrophilic DMA as the hydrophilic block on account of its simple chain structure, and hexyl acrylate (HA) for the hydrophobic component due to its commercial availability. We prepared nanoparticles using these monomers (**NP1**) and then introduced an azide bearing monomer (3-azidopropyl methacrylate monomer (AzPMA)) and acrylic acid (AA) monomer (**NP2**) to be able to both functionalize these nanoparticles through the azide moieties and stabilize their structure *via* crosslinking through the AA units (Figure 1).

2 | EXPERIMENTAL SECTION

2.1 | Materials

3-Chloropropanol (Sigma-Aldrich, 98%), sodium azide (NaN_3, Sigma-Aldrich, ≥99%), tetrabutylammonium bisulfate (Sigma-Aldrich, ≥99%), triethylamine (Alfa Aesar, 99%), methacryloyl chloride (Sigma-Aldrich, 97%, contains ~200 ppm monomethyl ether hydroquinone as stabilizer), hydroquinone (Sigma-Aldrich, ≥99%) were used as received. Hexyl acrylate (HA, Sigma-Aldrich, 99%), *N*,*N*-dimethyl acrylamide (DMA, Sigma-Aldrich, 99%), methyl methacrylate (MMA, Sigma-Aldrich, 99%), acrylic acid (anhydrous, contains 200 ppm MEHQ as inhibitor, 99%) and 1,4-dioxane (Sigma-Aldrich, 99.8%) were filtered through basic alumina prior to use. Poly(ethylene glycol) methyl ether (mPEG, Sigma-Aldrich, $M_n = 5000$ Da) 1,3,5-trioxane (Sigma-Aldrich, ≥99%), potassium persulfate (KPS, Sigma-Aldrich), 3-(trimethylsilyl)-1-propanesulfonic acid sodium salt (TMS, Sigma-Aldrich, 97%), *N*-(3-dimethylaminopropyl)-*N*′-ethylcarbodiimide hydrochloride (EDC.HCl, Sigma-Aldrich), cystamine dihydrochloride (Alfa Aesar, ≥97%), dibenzocyclooctyne-N-hydroxysuccinimidyl ester (DBCO-NHS, Sigma-Aldrich), *N*-ethyldiisopropylamine (DIPEA, Sigma Aldrich, ≥97%), *N*,*N*-dimethylformamide (DMF, Sigma-Aldrich), Fmoc-Trp(Boc)-OH (W, Sigma-Aldrich, ≥97%), Fmoc-Arg(PBF)-OH (R, Sigma-Aldrich), Rink Amide AM Resin (100–200 mesh) (VWR International), Oxyma Pure (Sigma-Aldrich), *N*,*N*′-diisopropylcarbodiimide (DIC, Sigma-Aldrich, 99%), piperidine (Alfa Aesar, 99%), trifluoroacetic acid (TFA, Sigma-Aldrich, 99%), 2,2′-(ethylenedioxy)diethanethiol (DODT, Sigma-Aldrich, 95%), triethylsilane (TES, Sigma-Aldrich, 97%) were used as received. 2,2′-Azobis(2-methylpropionitrile) (AIBN) was received from Molekula, recrystallized from methanol, and stored at 4 °C. 3-Azidopropyl methacrylate monomer (AzPMA) was prepared according to a previously described procedure.[38] mPEG chain transfer agent (mPEG-CTA) was synthesized following a previously described procedure.[39]

2.2 | Characterization

Nuclear magnetic resonance (^{1}H-NMR) spectra were recorded at 300 MHz on a Bruker DPX-300 spectrometer, using chloroform-d ($CDCl_3$) as the solvent. Chemical shifts of protons are reported as δ in parts per million (ppm) and are relative to solvent residual peaks.

Size exclusion chromatography (SEC) analysis was performed on a system composed of an Agilent 1260 Infinity II LC system equipped with an Agilent guard column (PLGel 5 μM, 50 × 7.5 mm) and two Agilent Mixed-C columns (PLGel 5 μM, 300 × 7.5 mm). The mobile phase used was $CHCl_3$ (HPLC grade) containing 0.5% v/v NEt_3 at 40 °C with a flow rate of 1.0 mL min^{-1} (poly(methyl methacrylate) (PM) standards were used for calibration). Detection was conducted using a differential refractive index (RI) detector. Number-average molecular weights (M_n), weight-average molecular weights (M_w) and dispersities ($Đ_M = M_w/M_n$) were determined using the Agilent GPC/SEC software.

High pressure liquid chromatography (HPLC) analyses were performed on a modular Shimadzu instrument

with the following modules: CBM-20A system controller, LC-20 AD solvent delivery module, SIL-20 AC HT autosampler, CTO-20 AC column oven, SPD-M20A photodiode array UV–Vis detector, RF-20A spectrofluorometric detector and a FRC-10 fraction collector. Chromatography was performed on a Shim-pack GISS 5 μm C18 (4.6 × 125 mm) reversed phase column heated at 30 °C. Flow rate was set at 0.8 mL·min^{-1} and the products eluted using a gradient of buffers: Buffer A: [H_2O (18.2 MΩ·cm^{-1} + 0.1 vol% Formic acid)]; Buffer B: [MeCN (HPLC grade) + 0.1 vol% Formic acid]. The elution of sequences with a tryptophan fluorophore was determined using the fluorescence detector (excitation wavelength 350 nm and emission wavelength 450 nm). The elution of sequences with dansyl fluorophore was determined using the fluorescence detector (excitation 335 nm and emission wavelength 519 nm).

Fourier Transform Infrared Spectroscopy was carried out using an Agilent Technologies Cary 630 FTIR spectrometer. Sixteen scans from 600 to 4000 cm^{-1} were taken at a resolution of 4 cm^{-1}, and the spectra were corrected for background absorbance.

Hydrodynamic diameters (DH) and size distributions (PD) of nano-objects were determined by dynamic light scattering (DLS) using a Malvern Zetasizer Nano ZS with a 4 mW He-Ne 633 nm laser module operating at 25 °C. Measurements were carried out at an angle of 173° (back scattering), and results were analyzed using Malvern DTS v7.03 software. All determinations were repeated 3 times with at least 10 measurements recorded for each run. DH values were calculated using the Stokes-Einstein equation, where particles are assumed to be spherical.

Dry-state-stained transmission electron microscopy (TEM) imaging was performed on a JEOL JEM-1400 microscope operating at an acceleration voltage of 80 kV. All dry state samples were diluted with deionized water to appropriate analysis concentration and then deposited onto formvar-coated or GO-coated copper grids. After roughly 1 min, excess sample was blotted from the grid and the grid was stained with an aqueous 1 wt% uranyl acetate (UA) solution for 1 min prior to blotting, drying and microscopic analysis.

2.3 | mPEG-*b*-P(DMA-*co*-HA)$_{99}$ nanoparticle (NP1) synthesis

mPEG-CTA (107 mg, 0.02 mmol), DMA (84 μL, 0.8 mmol), HA (215 μL, 1.2 mmol), KPS (1.8 mg, 7 × 10^{-3} mmol) were placed in a vial with a rubber septum, and DI water (0.250 g) was added to achieve a 10 w/w % solids concentration. TMS (89 mg, 0.4 mmol) was used as the internal standard. The solution was deoxygenated by purging with N_2 for 30 min, then placed in a heating block at 50 °C and left to stir overnight. After the reaction was complete, the vial was opened to the atmosphere while still in the heating block and subsequently stirred for 30 min to ensure reaction quenching. Samples were taken before and after the polymerization reaction to determine the conversion using ^{1}H NMR spectroscopy. A high monomer conversion of ≈99% was determined due to the disappearance of the DMA and HA vinyl signals at 5.78, 6.11, and 6.70 ppm (^{1}H NMR). Also, apparent HA signals at 4.0 ppm (-CH-$(CH_3)_2$) were detected. Particle size was measured by DLS at a temperature range of 50 °C-RT by using the sample taken from the polymerization solution while the solution was still at 50 °C.

2.4 | Synthesis of 3-azidopropyl methacrylate (AzPMA) monomer

3-Chloropropanol (10.6 mL, 12 g, 0.127 mol) was added to a mixture of water (15 mL), sodium azide (16 g, 0.254 mol, 2 equivalent), and tetrabutylammonium hydrogen sulfate (0.5 g). The mixture was stirred at 80 °C for 24 h and then at room temperature for 14 h. The product was extracted with ether (3 × 50 mL), the resulting solution was dried over sodium sulfate, the solvent was removed on a rotary evaporator to obtain 3-azidopropanol (yield: 7.3 g, 57%).

A solution of 3-azidopropanol (7.3 g, 0.072 mol), triethylamine (12.9 mL, 0.092 mol, dried over sodium sulfate), hydroquinone (0.05 g), and dichloromethane (DCM) (30 mL, dried over sodium sulfate) was cooled in an ice-water bath. Methacryloyl chloride (8.9 g, 8.4 mL, 0.09 mol) was added dropwise over a period of 20 min, and the mixture was stirred in the cooling bath for 1 h and then at room temperature for 14 h (Scheme 1). DCM (15 mL) was added, and the mixture was extracted with an aqueous solution of hydrochloric acid (1/10 v/v, 2 × 30 mL), water (2 × 30 mL), 10 wt % aqueous NaOH

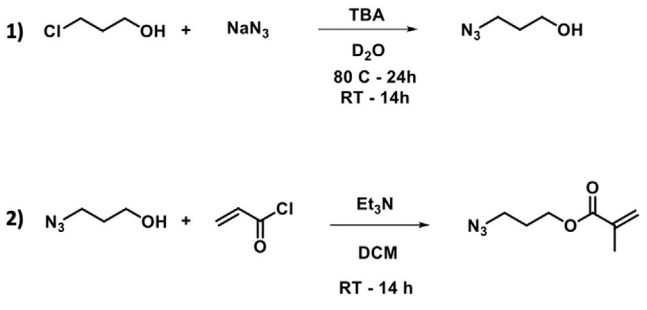

SCHEME 1 Synthesis of 3-azidopropyl methacrylate (AzPMA) monomer.

(2 × 30 mL), and again with water (2 × 30 mL). The DCM solution was mixed with hydroquinone (0.1 g) and dried over sodium sulfate. The organic solvent was removed under reduced pressure. The crude oil was purified by silica gel column chromatography (hexane: ethyl acetate, 4:1), resulting in a colorless oil.

2.5 | mPEG-*b*-P(AzPMA)$_1$-*b*-P(AzPMA-*co*-AA)$_2$ macro-CTA synthesis

Copolymerization of AzPMA monomer with acrylic acid (AA) was conducted starting with the polymerization of AzPMA by using AIBN as the initiator, mPEG-CTA as the RAFT agent, 1,3,5-trioxane as an internal reference, and 1,4-dioxane as the solvent, following the addition of AA monomer after achieving the targeted total DP of 1 to 5 with a molar ratio of [Monomer]/[1,3,5-Trioxane]/[mPEG-CTA]/[AIBN] = 10:20:1:0.1 in 1,4-dioxane (monomer/1,4-dioxane = 1:2 by volume) (Scheme 2).

For the synthesis of a copolymer: a stock solution of 10 mg mL^{-1} AIBN was prepared in 1,4-dioxane and 47 μL of this solution (0.5 mg, 2.8 × 10^{-3} mmol, 0.1 eq) was added to a vial of mPEG-CTA (150 mg, 2.8 × 10^{-2} mmol, 1.0 eq), AzPMA monomer (24 mg, 0.1 mmol, 5.0 eq), and 1,3,5-trioxane (51 mg, 5.7 × 10^{-1} mmol, 20 eq) in 1,4-dioxane and mixed in an oven-dried ampoule containing a magnetic stir bar until all solids dissolved. The resulting solution was degassed using at least three freeze-pump-thaw cycles, back-filled with N_2, and placed in a preheated oil bath at 70 °C. Samples were taken periodically to determine the overall and relative conversion of AzPMA. Meanwhile, AA (6.2 mg, 8.5 × 10^{-2} mmol, 3.0 eq) was purged with N_2 in a separate vial for 30 min. When 1 DP of AzPMA was achieved, AA was added to the reaction vessel under N_2. Once 1 DP of AA was achieved, the polymerization reaction was quenched by opening the vial to the air. Purification was achieved by dialysis (3–4 kDa MWCO) against 0.5–1 L nanopure water for 3 days with at least 6 water changes followed by lyophilization.

2.6 | mPEG-*b*-P(AzPMA)$_1$-*b*-P(AzPMA-*co*-AA)$_2$-b-P(DMA-*co*-HA)$_{99}$ nanoparticle (NP2) synthesis

For the synthesis of mPEG-*b*-P(AzPMA)$_1$-*b*-P(AzPMA-*co*-AA)$_2$-b-P(DMA-*co*-HA)$_{99}$ nanoparticle (Scheme 3), as a first step, in a vial with a rubber septum, P2 (67 mg, 0.01 mmol), DMA (46 μL, 0.4 mmol), HA (118 μL, 0.7 mmol), KPS (1.0 mg, 4 × 10^{-3} mmol) were added; DI water (1.94 g) was added to achieve a 10 w/w % solids concentration. TMS (49 mg, 0.2 mmol) was also added as an internal standard. The solution was deoxygenated by purging with N_2 for 30 min, then placed in a heating block at 50 °C and left to stir overnight. To quench the reaction, the vial was opened to the atmosphere while still in the heating block and stirred further for 30 min. Samples were taken before and after the polymerization reaction to determine the conversion using ^{1}H NMR spectroscopy. Particle size was measured on DLS at a temperature range of 50 °C to RT using the sample taken from the polymerization solution while the solution was still at 50 °C.

Secondly, EDC (5.9 mg, 0.03 mmol) was added to the reaction vessel while the quenched reaction vial was still in the heating block. After 30 min, cystamine hydrochloride (1.8 mg, 0.008 mmol) was added, and the solution was left to stir overnight at 50 °C. The amount of EDC was calculated by using 2× excess theoretical moles of acrylic acid (0.015 mmol), calculated from the polymer composition (1 AA unit) and amount of macro-CTA added (0.012 mmol), while the amount of cystamine hydrochloride was calculated as 0.5 equivalents of theoretical moles of AA.

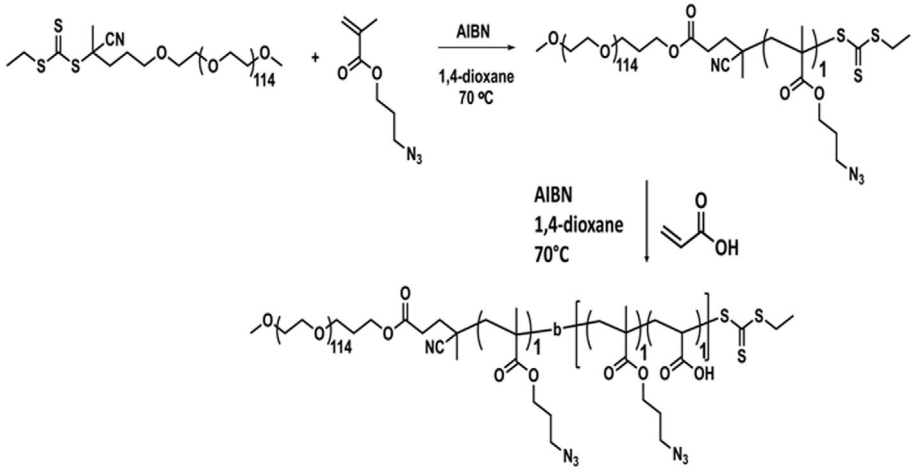

SCHEME 2 Synthetic scheme for the preparation of mPEG-*b*-P(AzPMA)$_1$-*b*-P(AzPMA-*co*-AA)$_2$ macro-CTA.

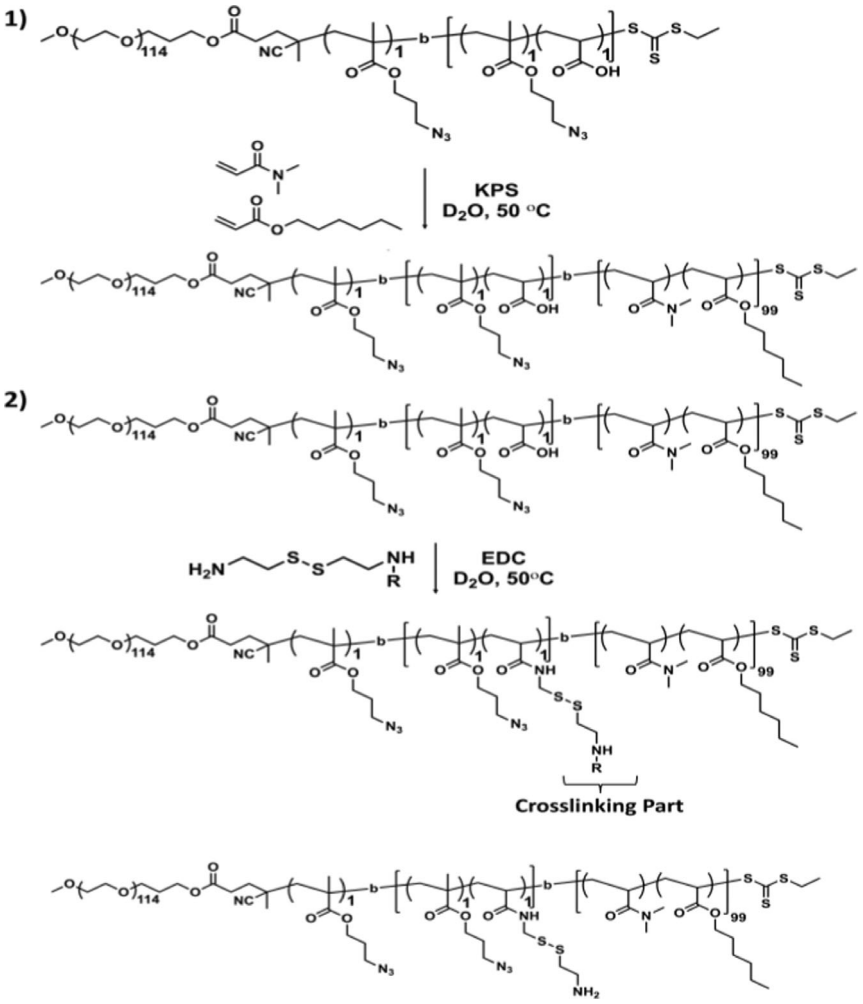

SCHEME 3 Synthetic scheme for the preparation of **(1)** mPEG-*b*-P(AzPMA)$_1$-*b*-P(AzPMA-*co*-AA)$_2$-b-P(DMA-*co*-HA)$_{99}$ nanoparticle (**NP2**) and **(2)** crosslinking of **NP2** through the acrylic acid units.

2.7 | Solid phase synthesis of $(WR)_3$ peptide

WRWRWR-NH_2, $(WR)_3$, peptide was synthesized on a microwave-assisted CEM Liberty Blue automated peptide synthesizer on a 0.25 mmol scale (Scheme 4).

Solutions of 0.2 M of amino acid, 1 M DIC and 1 M Oxyma were prepared in DMF and loaded onto the machine. Rink amide AM resin (0.78 mmol/g) was used for the synthesis of $(WR)_3$ peptide. 20% v/v piperidine solution in DMF was used as a deprotection solution. For Arginine, R, double coupling at 75 °C was carried out. After the synthesis, the resin was washed with DCM 3 times and the resulting peptide was cleaved from the resin by stirring at RT for 4 h in a cleavage solution of trifluoroacetic acid (TFA):2,2′-(ethylenedioxy)diethanethiol (DODT):triethylsilane (TES):H_2O with the ratio 92.5%:2.5%:2.5%:2.5%. After the cleavage, the resin was filtered, and the peptide was precipitated in cold diethyl ether 3 times and dried. $(WR)_3$ peptide was characterized by using mass spectroscopy and HPLC. Expected mass (Da): 1044.5760, Found mass (Da): 1044.5756 (Figure S1).

2.8 | $(WR)_3$ peptide conjugation to dibenzocyclooctyne-N-hydroxysuccinimidyl ester (DBCO-NHS)

DIPEA ((4 μL, 0.02 mmol, 2 eq) and DBCO-NHS (9.3 mg, 0.02 mmol, 2 eq) were added to the solution of $(WR)_3$ peptide (11.3 mg, 0.01 mmol, 1 eq) in DMF (1.2 mL), and the reaction mixture was stirred at RT for 8 h to obtain $(WR)_3$-DBCO-NHS conjugate (Scheme 5). $(WR)_3$-DBCO-NHS was precipitated in cold diethyl ether, collected by centrifugation, and dried under vacuum. The resulting conjugate was characterized by mass spectroscopy. Expected mass (Da): 1331.56, Found mass (Da): 1331.67 (Figure S2).

2.9 | Conjugation of $(WR)_3$-DBCO-NHS to NP2 via Cu-free click (SPAAC)

A solution of **NP2** (10 mg, 0.5×10^{-3} mmol, 1 eq) in DCM was added to the solution of $(WR)_3$-DBCO-NHS (2.1 mg, 0.2×10^{-3} mmol, 3 eq) in DMF and left to stir at RT for 24 h (Scheme 6). After the reaction, purification

was achieved by dialysis (3–4 kDa MWCO) against 0.5–1 L nanopure water for 3 days with at least 6 water changes followed by lyophilization. Resulting nanoparticles were characterized via FTIR, DLS and TEM.

3 | RESULTS AND DISCUSSION

3.1 | mPEG-*b*-P(DMA-*co*-HA)$_{99}$ nanoparticle (NP1) synthesis

We first prepared a polyethylene glycol chain transfer agent (mPEG CTA) (**P1**), and then carried out PITSA using DMA and HA as the core monomers to test the self-assembly behavior of the mPEG-*b*-P(DMA-*co*-HA) polymer. The CTA was synthesized following previous literature,[39] and then **P1** was obtained by 1-ethyl-3-(3-dimethylaminopropyl) carbodiimide (EDC) coupling with a commercial mPEG ($M_n = 5000$ Da) in the presence of catalytic 4-dimethylaminopyridine (DMAP). Successful synthesis was confirmed by ^{1}H NMR spectroscopy, and size-exclusion chromatography (SEC) confirmed that the mPEG-CTA had a monomodal and narrow molecular weight distribution (MWD) (Figure S3).

Using **P1**, PITSA of DMA and HA was conducted in water at 50 °C to obtain nanoparticles (**NP1**) (Figure 2A). The final molar composition of the purified copolymer was determined using ^{1}H NMR spectroscopy, and the molecular weight distribution (MWD) of the final copolymer was determined using size-exclusion chromatography (SEC). While quantitative blocking efficiency was not achieved for this copolymer (Figure S4), DLS analysis at 50 °C confirmed that this polymer could successfully form nanoparticles. Next, DLS measurements were carried out as a temperature ramp in the range of 20–50 °C (Figure S5, Table S2). DLS was used to characterize the dispersity (PDI = 0.25 at 50 °C) (Figure 2B) and the disassembly of these particles as the temperature was decreased below 50 °C (Figure 2C). This data confirmed that particle formation was driven by LCST behavior.

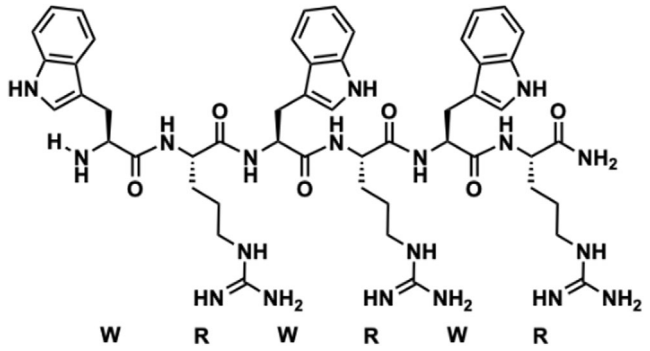

SCHEME 4 Structure of WRWRWR-NH$_2$, (WR)$_3$, peptide.

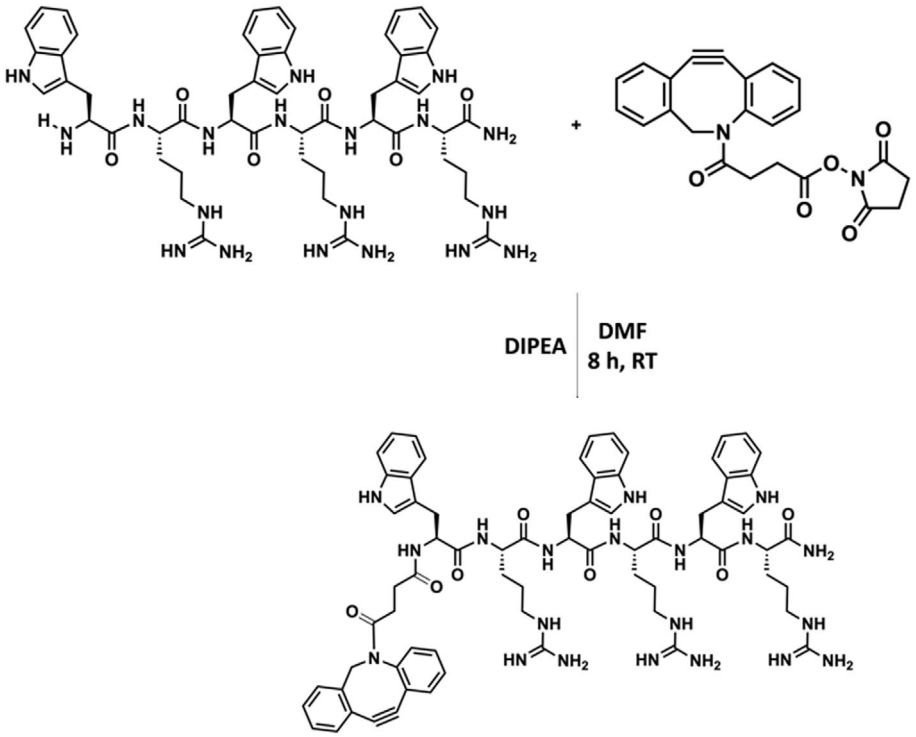

SCHEME 5 Synthetic scheme for the conjugation of (WR)$_3$ to dibenzocyclooctyne-*N*-hydroxysuccinimidyl ester (DBCO-NHS).

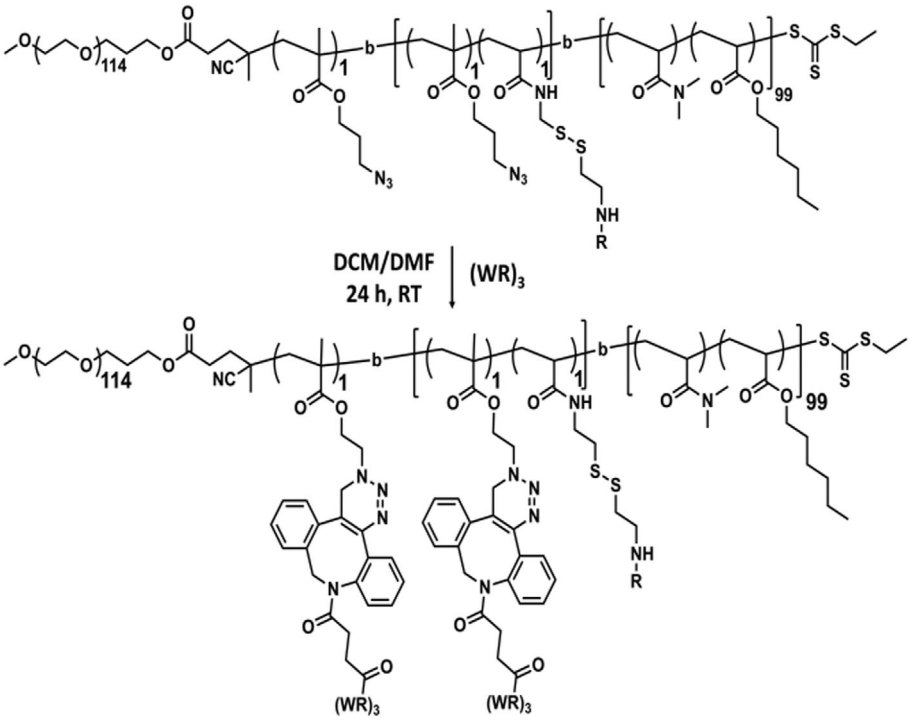

SCHEME 6 Synthetic scheme for the conjugation of $(WR)_3$-DBCO-NHS to **NP2** via Cu-free Click (SPAAC).

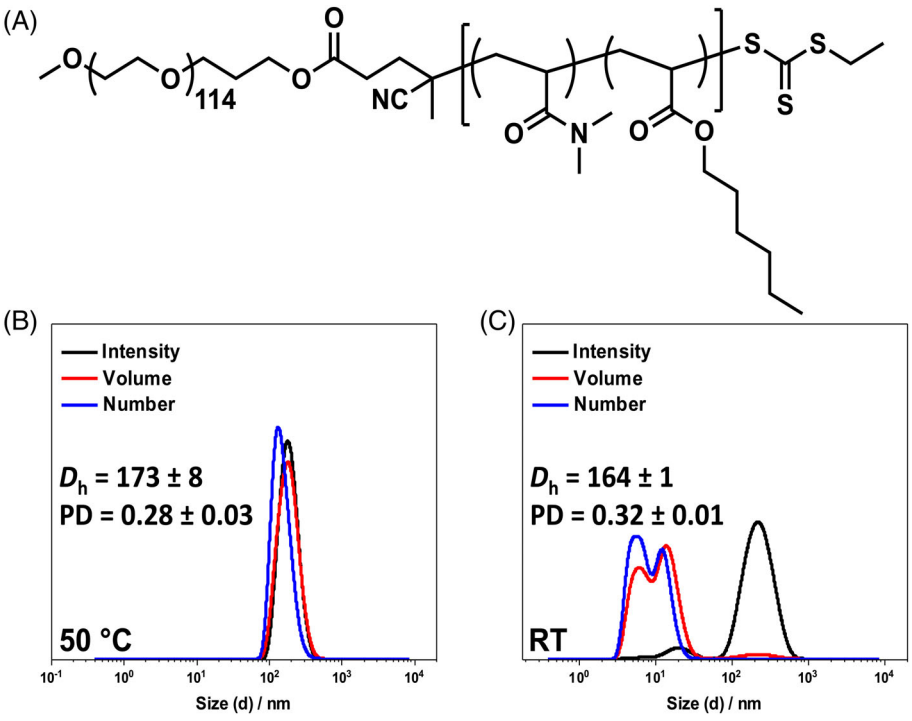

FIGURE 2 (A) Structure of **NP1** nanoparticles. Size distribution and polydispersity index of **NP1** (B) at 50 °C and (C) at room temperature measured by DLS.

3.2 | mPEG-*b*-P(AzPMA)$_1$-b-P(AzPMA-*co*-AA)$_2$-*b*-P(DMA-*co*-HA)$_{99}$ nanoparticle (NP2) synthesis

With our PITSA system validated, we next wanted to investigate the ability to increase the functionality of the NP surface, for example to further attach therapeutic molecules or targeting agents. To this end, an azide-bearing monomer, azidopropyl methacrylate (AzPMA), was introduced into the polymer to enable post-polymerization functionalization through azide-alkyne cycloaddition. A small fraction of acrylic acid (AA) units was also introduced into the polymer structure to enable core crosslinking of the resulting nanoparticles to prevent

their disassembly, allowing characterization of the nanoparticles at room temperature (RT). AA was introduced after the first block was polymerized to a certain AzPMA monomer DP, given that the AA has a higher reaction rate than AzPMA.

First, the azidopropyl methacrylate (AzPMA) monomer was synthesized from 3-azidopropanol (AzPOH) (see supporting information for detailed procedure) and characterized by ^{1}H NMR spectroscopy (Figure S6). Then, the macro-CTA was synthesized by polymerization of AzPMA at 70 °C with the sequential addition of AA. AzPMA conversion was monitored by ^{1}H NMR spectroscopy, and AA was added when 1 DP of AzPMA monomer had been obtained (Figure S7). The MWD for the mPEG-*b*-P(AzPMA)$_1$-*b*-P(AzPMA-*co*-AA)$_2$ copolymer (**P2**) was determined using SEC, which showed a slightly higher dispersity ($Đ_M$) of 1.32 (Figure S8). Next, PITSA of DMA and HA was conducted using **P2** in water to yield azide-functionalized nanoparticles (**NP2**). PITSA of DMA and HA using **P2** was carried out at 50 °C as with **NP1**. We expected that **P2** would have a lower LCST than **P1**, as our previous research indicates that the hydrophobic AzPMA would have a greater effect than hydrophilic AA on the overall copolymer hydrophobicity.

To better explain the effect of monomer hydrophobicity, partition coefficients (Log*P*), which are used to determine the hydrophobicity of small molecules, were used to calculate the hydrophobicity of both monomers using ChemBio 3D. Log*P* was calculated as 2.49 for AzPMA and 0.35 for AA, showing that AzPMA is more hydrophobic than AA. This suggests that the overall copolymer would be more hydrophobic as there are more AzPMA units than the AA monomer in the final copolymer. As such, it is likely to undergo a phase transition at a lower temperature than for **P1**.

To characterize the block copolymer assemblies at room temperature after the PITSA process, cystamine was added to the **NP2** polymerization solution at 50 °C to crosslink through the acid groups of AA *via* EDC coupling. The final composition of the polymers after PITSA was determined *via* ^{1}H NMR spectroscopy, which confirmed a final composition of mPEG-*b*-P(AzPMA)$_1$-*b*-P(AzPMA-*co*-AA)$_2$-*b*-P(DMA-*co*-HA)$_{99}$. SEC analysis showed a broad distribution with high $Đ_M$ of 2.90 due to the swelling of the nanoparticles when dispersed in $CHCl_3$ (SEC solvent) (Figure S9). The formation of particles was tracked via DLS measurements during a temperature ramp in the range of 20–50 °C (Figure S10, Table S3). As with **NP1**, when **NP2** was uncrosslinked (Figure 3A), particles could be observed at 50 °C followed by particle disassembly with decreasing temperature (Figure 3B). Following the crosslinking reaction, DLS measurements were repeated over the same temperature range (Figure S11, Table S4). As shown in Figure 3C below, successful crosslinking was confirmed by the presence of stable particles at both 50 °C and RT. This was further demonstrated by TEM analysis which showed stable particles with a size of approximately 42 nm. The difference in sizes between DLS and dry-state TEM measurements were attributed to the drying effect as TEM images the dry particles whereas DLS measures the hydrodynamic volume of the particles in solution (Figure 3C).

3.3 | Conjugation of $(WR)_3$-DBCO-NHS to NP2 via Cu-free click (SPAAC)

As a next step, we investigated how post-polymerization functionalization of the particles would affect their stability. To this end, we attached a short antibacterial peptide containing tryptophan (W) and arginine (R) amino acids, $(WR)_3$, through the azide units on the surface of **NP2**. It has been reported that the $(WR)_3$ peptide shows good antibacterial efficiency against widely used bacterial strains.[40] Based on this, this peptide was selected as a functionalizing agent for the synthesized nanoparticles to create antimicrobial therapeutic NPs.

First, the antibacterial peptide $(WR)_3$ was synthesized *via* solid phase peptide synthesis (SPPS) on an automated peptide synthesizer. The peptide was obtained with 90% purity which was determined using HPLC (Figure S12). Then, the $(WR)_3$ peptide was reacted with dibenzocyclooctyne-*N*-hydroxysuccinimidyl ester (DBCO-NHS) to enable attachment with the crosslinked **NP2** via copper-free Click chemistry (SPAAC) through the azide units (Figure 4A). ^{1}H NMR spectroscopy did not provide distinguishable peaks, and therefore attachment of the peptide was confirmed via Fourier Transform Infrared (FTIR) spectroscopy, with the formation of a peak at 1997 nm^{-1} from the C=N bonds of peptide side chains on the spectra of **NP2**-$(WR)_3$ (Figure S13). It should be noted that the disappearance of the azide peak upon attachment could not be monitored as both **NP2** and $(WR)_3$ peptides displayed the same signal on their FTIR spectra at the same region where the azide peak is found.

Next, the stability of the peptide-functionalized nanoparticles was determined using DLS and TEM. DLS results showed particle formation with a good correlation curve, and TEM images further confirmed that **NP2** was stable after functionalizing with the $(WR)_3$ peptide. The size of the particles after $(WR)_3$ attachment was found to be smaller according to the DLS and TEM results (Figure 4B). We attribute this to the nanoparticle hydrophobicity increasing with $(WR)_3$ attachment, due to the

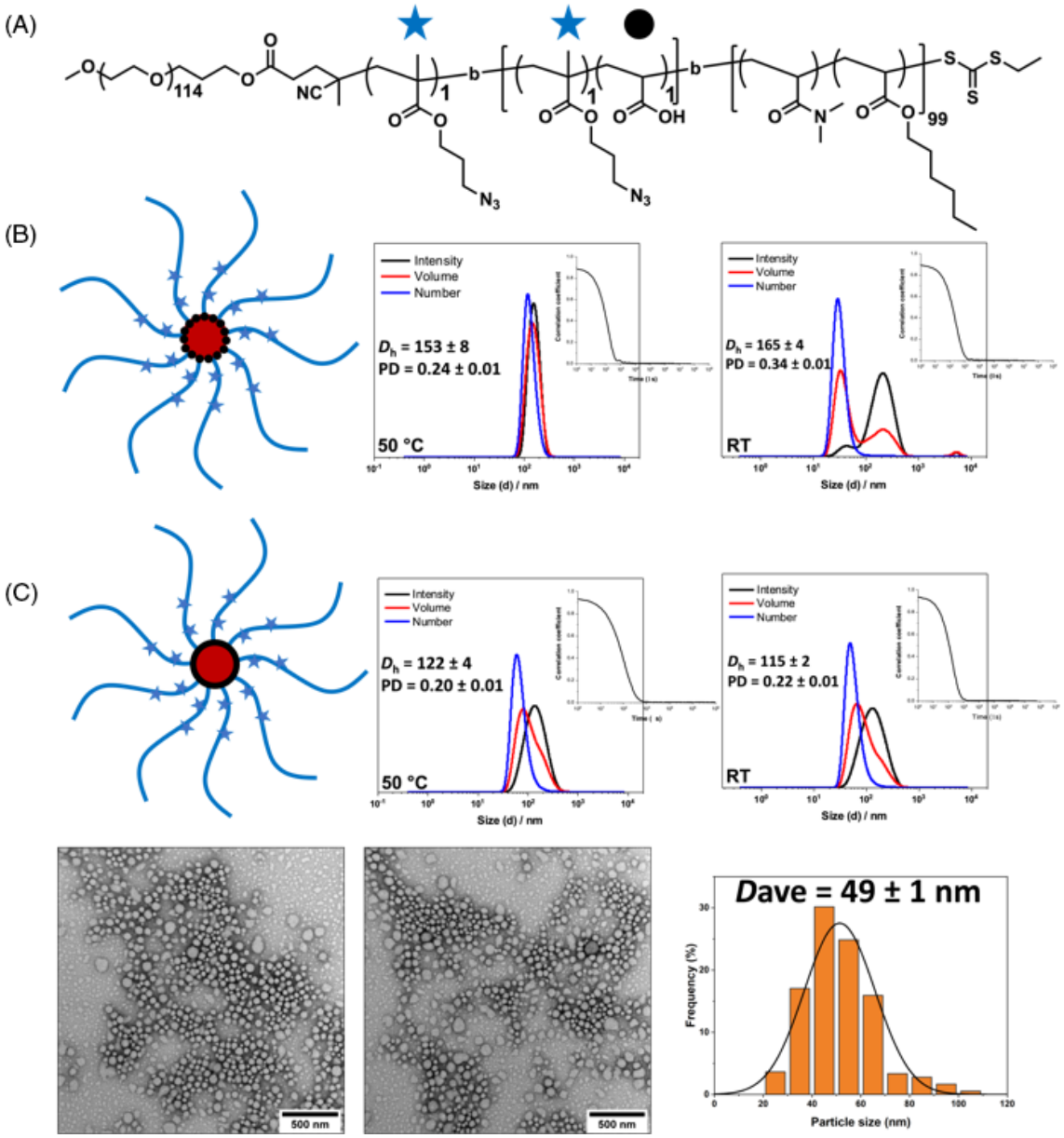

FIGURE 3 (A) Chemical structure of mPEG-*b*-P(AzPMA)$_1$-b-P(AzPMA-*co*-AA)$_2$-*b*-P(DMA-*co*-HA)$_{99}$ nanoparticle (**NP2**) (star and ball representing the AzPMA and AA monomers, respectively) and (B) size distribution and polydispersity index for uncrosslinked **NP2** at 50 °C and at RT and (C) size distribution and polydispersity index for crosslinked **NP2** at 50 °C and at RT measured by DLS and corresponding TEM images.

increased interactions with the polymer chains causing shrinking of the particles.

We lastly performed proof-of-concept antimicrobial assays to assess the therapeutic potential of the peptide-labeled NPs. A preliminary test for the antibacterial activity of the $(WR)_3$ peptide, **NP2** and **NP2**-$(WR)_3$ nanoparticles was carried out against *Staphylococcus aureus* bacteria. Each sample was incubated with bacteria cultured in 200 μL of Luria-Bertani broth (LB broth) at concentrations of 200, 150, 100, 75, 50, 25, 10. 7.5, 5.0, 2.5, 1 and 0 μg/mL. The results confirmed that the $(WR)_3$ peptide had antimicrobial activity against the *S. aureus* bacteria, and that this antimicrobial activity was maintained after being conjugated to the polymer particles (Figure S14). Further, there was a large increase in the antimicrobial activity of the functionalized **NP2**-$(WR)_3$ in comparison to the plain **NP2,** acting as confirmation of successful peptide attachment. Further antimicrobial tests are warranted to precisely determine the antibacterial activity of the nanoparticles by altering the dose of NPs against the bacteria.

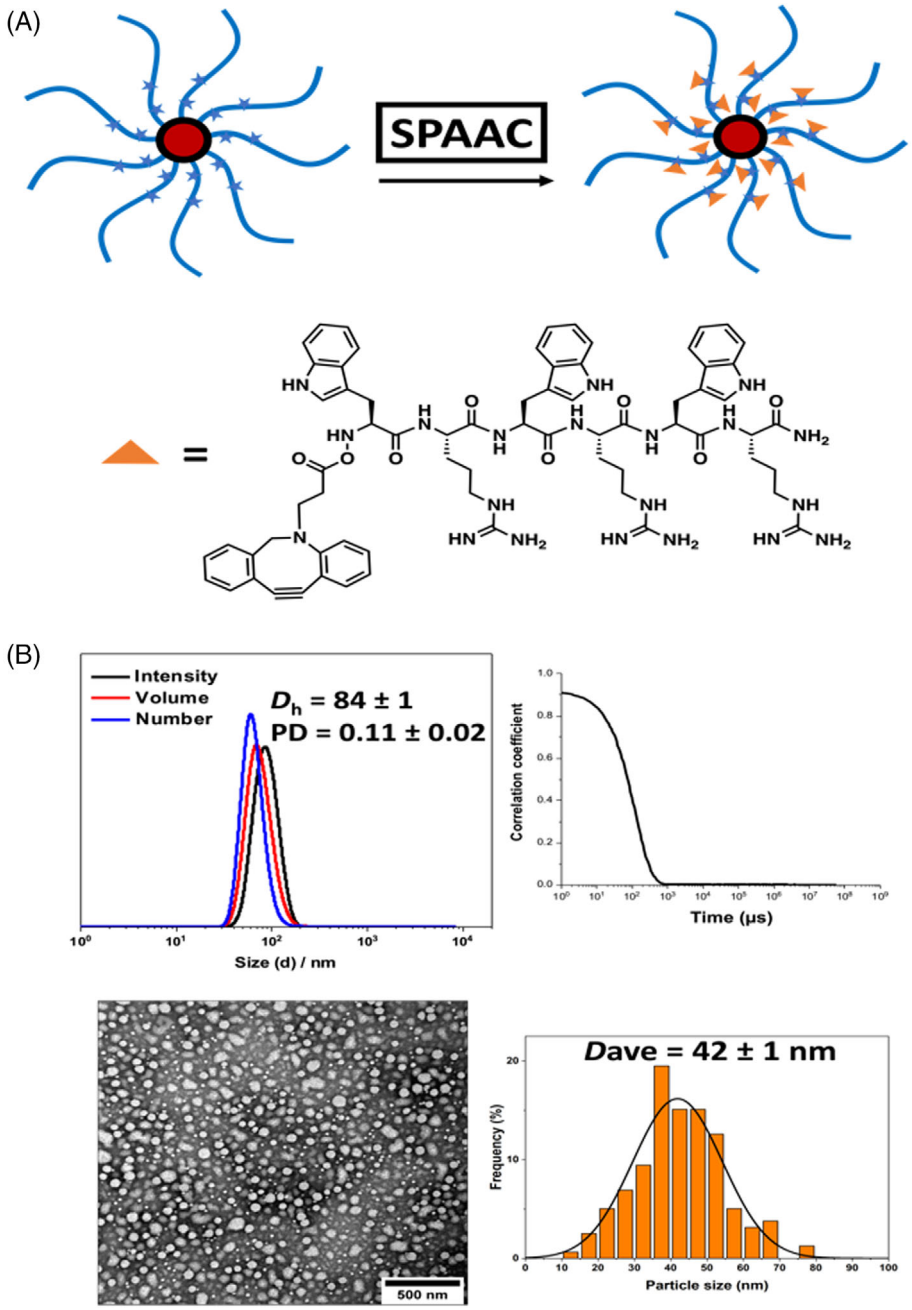

FIGURE 4 (A) Schematic representation of $(WR)_3$ peptide attachment to **NP2** via SPAAC. (B) Size distribution and polydispersity index of $(WR)_3$-**NP2** particles measured by DLS and accompanying TEM image.

4 | CONCLUSION

Notably, after showing in our previous work that polymers based on monomers known to produce non-responsive homopolymers can yield thermoresponsive copolymers, we have demonstrated in this work that these copolymers can also form nanoparticles upon the thermal trigger. This is a promising development which will enable the design of new thermoresponsive nanoparticles with tunable temperature responses upon varying the constituent polymer chemistries. These results confirm that PITSA is an efficient method for the preparation and functionalization of nanoparticles with inherent thermoresponse. We have further demonstrated that PITSA nanoparticles can find application in various areas as they are amenable to functionalization with fluorescent dyes, antibodies, anticancer drugs *etc*. Additionally, nanoparticles with different morphologies that can be achieved *via* PITSA can be functionalized by introducing various moieties into the polymer structure, allowing the building of diverse libraries of functional nanoparticles with different morphologies.

To conclude, we report the synthesis of thermoresponsive copolymers of DMA and HA monomers *via* PITSA and investigate their self-assembly behavior by measuring the particle size using DLS. The results

showed that both simple mPEG-*b*-P(DMA-*co*-HA) and azide functionalized mPEG-*b*-P(AzPMA)-*b*-P(AzPMA-*co*-AA)-*b*-P(DMA-*co*-HA) copolymers assemble to form nanoparticles at 50 °C, and they disassemble below that temperature unless they are core crosslinked through acrylic acid units. We also demonstrated that these nanoparticles could be functionalized with short antibacterial peptides while maintaining their stability, showing promising antibacterial activity and as such, posing as a nanoparticle platform that can be functionalized to bear various moieties.

Our next steps are to further test the antimicrobial efficiency of the $(WR)_3$ peptide, the plain nanoparticles, and the peptide-attached nanoparticles to determine minimum inhibitory concentration (MIC) values. This study can also be expanded to investigate the antibacterial activity of the obtained functionalized nanoparticles against other common bacteria strains such as *Escherichia coli*.

Overall, this study demonstrates that various functional nanoparticles can be prepared using PITSA and these systems hold potential for various therapeutic applications. We envisage that the diversification of monomers used for PITSA will allow the design of tailored nanoparticles with tunable properties for targeting different applications.

ACKNOWLEDGMENTS

This work is supported by the Turkish Ministry of National Education; the Engineering and Physical Sciences Research Council, EPSRC, (EP/S00338X/1), and the University of Birmingham. The authors would like to thank Ms. Bethany Crow for her assistance with HPLC measurements and Ms. Alisha Miller for her assistance with the TEM images. C. M. S. K. was a Researcher Co-Investigator in the Biotechnology and Biological Sciences Research Council Responsive mode grant (BB/S017526/1).

FUNDING INFORMATION

EPSRC and University of Birmingham.

ORCID

Amanda K. Pearce https://orcid.org/0000-0003-3372-7380
C. M. Santosh Kumar https://orcid.org/0000-0002-1370-2365
Calum Ferguson https://orcid.org/0000-0002-6168-4624
Rachel K. O'Reilly https://orcid.org/0000-0002-1043-7172

REFERENCES

[1] D. Li, R. Zhang, G. Liu, Y. Kang, J. Wu, *Adv. Healthc. Mater.* **2020**, *9*(20), 2000605.
[2] N. Narayan, A. Meiyazhagan, R. Vajtai, *Materials* **2019**, *12*(21), 3602.
[3] Z. Nie, A. Petukhova, E. Kumacheva, *Nat. Nanotechnol.* **2010**, *5*(1), 15.
[4] J. Tan, C. Huang, D. Liu, X. Li, J. He, Q. Xu, L. Zhang, *ACS Macro Lett.* **2017**, *6*(3), 298.
[5] Z. Li, J. Ding, M. Day, Y. Tao, *Macromolecules* **2006**, *39*(7), 2629.
[6] L. Yang, J. Tang, H. Yin, J. Yang, B. Xu, Y. Liu, Z. Hu, B. Yu, F. Xia, G. Zou, *Sci. Eng.* **2022**, *8*(2), 880.
[7] B. Charleux, G. Delaittre, J. Rieger, F. D'Agosto, *Macromolecules* **2012**, *45*(17), 6753.
[8] C. Liu, C.-Y. Hong, C.-Y. Pan, *Polym. Chem.* **2020**, *11*(22), 3673.
[9] Y. Mai, A. Eisenberg, *Chem. Soc. Rev.* **2012**, *41*(18), 5969.
[10] J. C. Foster, S. Varlas, B. Couturaud, Z. Coe, R. K. O'Reilly, *J. Am. Chem. Soc.* **2019**, *141*(7), 2742.
[11] N. J. W. Penfold, J. Yeow, C. Boyer, S. P. Armes, *ACS Macro Lett.* **2019**, *8*(8), 1029.
[12] J. C. Foster, S. Varlas, B. Couturaud, J. R. Jones, R. Keogh, R. T. Mathers, R. K. O'Reilly, *Am. Ethnol.* **2018**, *130*(48), 15959.
[13] H.-J. Huang, Y.-L. Tsai, S.-H. Lin, S.-H. Hsu, *J. Biomed. Sci.* **2019**, *26*, 1.
[14] O. Bertrand, J.-F. Gohy, *Polym. Chem.* **2017**, *8*(1), 52.
[15] G. Kocak, C. Tuncer, V. Bütün, *Polym. Chem.* **2017**, *8*(1), 144.
[16] P.-H. Hsu, A. Almutairi, *J. Mater. Chem. B* **2021**, *9*(9), 2179.
[17] R. Hoogenboom, in *Smart Polymers and their Applications (Second Edition)* (Eds: M. R. Aguilar, J. San Román), Woodhead Publishing, Duxford **2019**, p. 13.
[18] P. Schattling, F. D. Jochum, P. Theato, *Polym. Chem.* **2014**, *5*(1), 25.
[19] J. Bergueiro, M. Calderón, *Macromol. Biosci.* **2015**, *15*(2), 183.
[20] F. Doberenz, K. Zeng, C. Willems, K. Zhang, T. Groth, *J. Mater. Chem. B* **2020**, *8*(4), 607.
[21] A. P. Constantinou, L. Wang, S. Wang, T. K. Georgiou, *Polym. Chem.* **2023**, *14*(3), 223.
[22] S. R. Abulateefeh, S. G. Spain, J. W. Aylott, W. C. Chan, M. C. Garnett, C. Alexander, *Macromol. Biosci.* **2011**, *11*(12), 1722.
[23] M. T. Cook, P. Haddow, S. B. Kirton, W. J. McAuley, *Adv. Funct. Mater.* **2021**, *31*(8), 2008123.
[24] S. Phunpee, U. R. Ruktanonchai, S. Chirachanchai, *Biomacromolecules* **2022**, *23*(12), 5361.
[25] E. Kostyurina, J. U. De Mel, A. Vasilyeva, M. Kruteva, H. Frielinghaus, M. Dulle, L. Barnsley, S. Förster, G. J. Schneider, R. Biehl, et al., *Macromolecules* **2022**, *55*(5), 1552.
[26] T. Horiuchi, T. Sakai, Y. Sanada, K. Watanabe, M. Aida, Y. Katsumoto, *Langmuir* **2017**, *33*(51), 14649.
[27] X. Chen, T. Michinobu, *Macromol. Chem. Phys.* **2022**, *223*(1), 2100370.
[28] D. Pizzi, J. Humphries, J. P. Morrow, A. M. Mahmoud, N. L. Fletcher, S. E. Sonderegger, C. A. Bell, K. J. Thurecht, K. Kempe, *Biomacromolecules* **2022**, *24*(1), 246.
[29] E. A. Ksendzov, P. A. Nikishau, I. M. Zurina, V. S. Presniakova, P. Timashev, Y. A. Rochev, S. Kotova, S. V. Kostjuk, *ACS Applied Polymer Materials* **2022**, *4*(2), 1344.
[30] M. P. J. Miclotte, S. Varlas, C. D. Reynolds, B. Rashid, E. Chapman, R. K. O'Reilly, *ACS Appl. Mater. Interfaces.* **2022**, *14*(48), 54182.
[31] J.-F. Lutz, A. Hoth, *Macromolecules* **2006**, *39*(2), 893.

[32] Q. Li, L. Wang, F. Chen, A. P. Constantinou, T. K. Georgiou, *Polym. Chem.* **2022**, *13*(17), 2506.
[33] Q. Li, R. Wang, J. Lee, J. S. Correia, A. P. Constantinou, J. Krell, T. K. Georgiou, *Eur. Polym. J.* **2023**, *194*, 112144.
[34] I. Akar, R. Keogh, L. D. Blackman, J. C. Foster, R. T. Mathers, R. K. O'Reilly, *ACS Macro Lett.* **2020**, *9*(8), 1149.
[35] I. Akar, J. C. Foster, X. Leng, A. K. Pearce, R. T. Mathers, R. K. O'Reilly, *ACS Macro Lett.* **2022**, *11*(4), 498.
[36] C. A. Figg, A. Simula, K. A. Gebre, B. S. Tucker, D. M. Haddleton, B. S. Sumerlin, *Chem. Sci.* **2015**, *6*(2), 1230.
[37] M. Vakili, V. J. Cunningham, M. Trebbin, P. Theato, *Macromol. Chem. Phys.* **2019**, *220*(2), 1800370.
[38] B. S. Sumerlin, N. V. Tsarevsky, G. Louche, R. Y. Lee, K. Matyjaszewski, *Macromolecules* **2005**, *38*(18), 7540.
[39] X. Huang, S. I. Sevimli, V. Bulmus, *Eur. Polym. J.* **2013**, *49*(10), 2895.
[40] M. B. Strøm, B. E. Haug, M. L. Skar, W. Stensen, T. Stiberg, J. S. Svendsen, *J. Med. Chem.* **2003**, *46*(9), 1567.

SUPPORTING INFORMATION

Additional supporting information can be found online in the Supporting Information section at the end of this article.

How to cite this article: I. Akar, A. K. Pearce, C. M. S. Kumar, C. Ferguson, R. K. O'Reilly, *J. Polym. Sci.* **2023**, 1. https://doi.org/10.1002/pol.20230420